Journal of Power Sources 244 (2013) 280–286

Contents lists available at SciVerse ScienceDirect

Journal of Power Sources

journal homepage: www.elsevier.com/locate/jpowsour

Liquid phase co-exfoliated MoS_2–graphene composites as anode materials for lithium ion batteries

Viet Hung Pham [a], Kwang-Hyun Kim [b], Dong-Won Jung [a], Kuldeep Singh [a], Eun-Suok Oh [a], Jin Suk Chung [a,*]

[a] School of Chemical Engineering, University of Ulsan, 93 Daehakro, Ulsan 680-749, South Korea
[b] POSCO ESM, 217 Bongsan-Ri, Sandong-Myun, Gumi, Kyungbuk-Do 730-853, South Korea

HIGHLIGHTS

- MoS_2/graphene composites were prepared by liquid phase co-exfoliation.
- Thin flakes of exfoliated MoS_2 facilitate the access of Li^+ during lithiation.
- MoS_2/CCG shows good capacity, excellent cycling stability and high rate capacity.

ARTICLE INFO

Article history:
Received 5 October 2012
Received in revised form
28 November 2012
Accepted 9 January 2013
Available online 21 January 2013

Keywords:
Lithium ion battery
Molybdenum disulfide
Graphene nanoplatelet
Chemically converted graphene and composite

ABSTRACT

We report a facile method to prepare the MoS_2–graphene composites by liquid phase co-exfoliation of commercial MoS_2 with graphene nanoplatelet (GnP) and chemically converted graphene (CCG) in N-methyl pyrrolidone with the aid of ultrasonication. The combination of SEM, XRD and BET results reveal that the MoS_2–graphene composites are mesoporous materials consisting of very thin MoS_2 flakes and graphene sheets. The prepared MoS_2–graphene composites display good performance as anode materials for lithium ion batteries. Exfoliation of the MoS_2 is the key factor for high electrochemical lithiation/delithiation performance. The MoS_2/CCG composite exhibits the best reversible capacity (up to 750 mA h g^{-1} after 50 cycles), excellent cycling stability and high rate capability. The reversible capacity at a rate of 2000 mA g^{-1} is over 350 mA h g^{-1} and recovers to as high as 720 mA h g^{-1} at a rate of 100 mA g^{-1}.

1. Introduction

Lithium ion batteries (LIBs) are the leading power sources for portable electronic devices and are promising candidate power sources for electric vehicles due to their high energy density, light weight and long service life [1–4]. For conventional LIBs, graphite is widely used as the anode material because of its flat potential profile versus lithium and its structural stability during cycling. However, the low theoretical capacity of graphite makes it important to find alternative anode materials.

Recently, graphene-like structural molybdenum disulfide (MoS_2), a transition metal chalcogenide, has emerged as promising anode material for LIB with high capacity and excellent cyclic stability [5–11]. The weak van der Waals interaction between MoS_2 layers allows lithium ions to diffuse without a significant increase in volume expansion [8]. However, the reversible capacity of highly crystalline MoS_2 is quite low, only about 200 mA h g^{-1} [8,9]. Most attempts to improve the reversible capacity of MoS_2 focused on enlarging the interlayer distance or creating a disordered structure to relax the strain and lower the barrier for Li intercalation [8–11]. Du et al. [8] enlarged the interlayer distance of MoS_2 by exfoliation of lithiated MoS_2 in an aqueous solution via hydrolysis and then restacking of MoS_2 via hydrothermal treatment. The restacked MoS_2 exhibited a reversible capacity of 750 mA h g^{-1} after 50 cycles at a rate of 50 mA g^{-1}. To improve the enlarging efficiency, Xiao et al. [9] exfoliated lithiated MoS_2 in a poly(ethylene oxide) (PEO) solution by which PEO adsorbed on the surface of MoS_2 sheets was incorporated into the intersheet region of restacked MoS_2. The MoS_2/PEO exhibited a reversible capacity of more than 900 mA h g^{-1} after 50 cycles at a current density of 100 mA g^{-1}. Recently, Hwang et al. [11] reported that disordered MoS_2 synthesized by a solvothermal method possessed a significantly enlarged interlayer distance. The disordered

* Corresponding author. Tel.: +82 52 259 2249; fax: +82 52 2591689.
E-mail address: jschung@mail.ulsan.ac.kr (J.S. Chung).

0378-7753/$ – see front matter © 2013 Elsevier B.V. All rights reserved.
http://dx.doi.org/10.1016/j.jpowsour.2013.01.053

MoS_2 showed a reversible capacity of 912 mA h g^{-1} at a rate of 1 C and an excellent reversible capacity of 554 mA h g^{-1} even after 20 cycles at a current density of 50 C.

Graphene, a flat monolayer of carbon atoms packed into a two-dimensional honeycomb lattice, has attracted a great attention for energy storage applications due to its excellent electrical conductivity, large surface area, structural flexibility and chemical stability [12,13]. The specific capacity of graphene nanosheet was found to be 540 mA h g^{-1}, which is much larger than that of graphite [14,15]. However, the cyclic performance was poor as the capacity drops to 290 mA h g^{-1} after only 20 cycles. Currently, graphene is frequently used as host material for fast and efficient lithium storage. The combination of graphene with restacked MoS_2 yields a significant increase in reversible capacity and rate capacity [16–18]. By incorporation of only 2.0 wt% graphene to a MoS_2/POE composite, Xiao et al. [16] found that the rate capacity significantly increased. At rates as high as 10,000 mA g^{-1}, the reversible capacity of MoS_2/POE/graphene was over 250 mA h g^{-1}, whereas the reversible capacity of MoS_2/POE was less than 100 mA h g^{-1}. Chang et al. [17] *in situ* synthesized MoS_2–graphene composite by a hydrothermal method, which exhibited extraordinary capacity, up to 1300 mA h g^{-1}, and excellent rate capability and cycling stability.

According to Xiao et al. [9], although the mechanism is not clear, the reversible capacity of MoS_2 is strongly dependent on the morphology of MoS_2 particles. The commercial, highly crystalline MoS_2 exhibited a first discharge capacity of about 600 mA h g^{-1} but a fast decrease to 200 mA h g^{-1} in the second cycle, suggesting poor reversibility of Li^+ in the pristine MoS_2. Most of Li^+ ions are trapped in the unexfoliated structure after the first discharge [9]. Recently, Coleman et al. [19–23] demonstrated that layered materials such as graphite and MoS_2 are easily exfoliated to single and few-layered flakes by liquid-phase exfoliation in polar organic solvents. More interestingly, blending graphene and MoS_2 dispersions produced hybrid dispersions which can be filtrated into hybrid films [22].

The *in situ* synthesis usually resulted in the formation of amorphous MoS_2 [6,7,12,13,17,18]. Although amorphous MoS_2 can be converted to crystalline MoS_2 by thermal annealing, the obtained crystallinity is not very high. Since the crystallinity of materials plays a critical role in determining the performance of the electrode materials in LIBs [6], in this study, we tried to use commercial, highly crystalline MoS_2 to prepare composites with graphene nanoplates (GnPs) and chemically converted graphene (CCG). Taking advantage of liquid-phase exfoliation of MoS_2 and graphene in polar organic solvents under sonication condition, MoS_2–graphene composites were directly prepared by the co-exfoliation of MoS_2 and graphenes in N-methyl-pyrrolidone. We then used these composites as anode materials for LIBs. Exfoliation of bulk MoS_2 into single and few-layered flakes resulted in increasing surface area, facilitating the access of Li^+ ions to the electrode active material during the lithiation process. The MoS_2/CCG composite exhibited the best reversible capacity, up to 750 mA h g^{-1}, excellent cyclic stability and high rate performance.

2. Experimental

2.1. Materials

Expandable graphite (Grade 1721) was kindly provided by Asbury Carbon. GnP (xGnP® grade M) was purchased from XG Science. Concentrated sulfuric acid (H_2SO_4), potassium permanganate ($KMnO_4$), hydrochloric acid (HCl), hydrogen peroxide (H_2O_2) and N-methyl-pyrrolidone (NMP) were purchased from Samchun Chemicals. MoS_2 and hydrazine monohydrate were purchased from Sigma–Aldrich. All chemicals were used as received without further purification.

2.2. Chemically converted graphene synthesis

The as-synthesized graphene oxide was prepared by the modified Hummers method from expanded graphite, which was prepared by the microwave-assisted thermal expansion of expandable graphite [24]. CCG synthesis is described elsewhere [25]. Briefly, as-synthesized graphene oxide (10 mg mL^{-1}) was diluted with DMF to a concentration of 2 mg mL^{-1}, and was sonicated in an ultrasonic bath (Jeiotech UC-10, 200 W) for 1 h to create a homogenous suspension of graphene oxide in DMF–water (80:20 v/v). The hydrazine reduction was carried out by adding 10 mL hydrazine monohydrate (98%) to 200 mL of the graphene suspension under mixing at 40 °C for 24 h. The obtained CCG suspensions were filtered and washed copiously with DMF to remove excess hydrazine.

2.3. MoS_2–graphene composites preparation

Exfoliation of MoS_2 was carried out following Coleman's method [23]. Typically, 10 g of MoS_2 was dispersed in 100 mL NMP and the mixture was subjected to pulsed sonication under magnetic stirring for a total of 6 h using a horn probe sonic tip (VibraCell CVX, 750 W, 30% amplitude). All sonication processes mentioned in this paper were done with 45 s pulse on and 15 s pulse off cycles under ice cooling. The resulting dispersion was centrifuged at 1000 rpm for 1 h and the supernatant containing MoS_2 single and few-layered flakes was collected and retained for use. To determine the concentration, 5 mL MoS_2 dispersion was coagulated in methanol, filtered, dried at 100 °C for 3 h and weighed to calculate the concentration, which was about 3.0 mg mL^{-1}.

Graphene dispersions were prepared by dispersing CCG filtered cake and GnP in NMP at the concentration of 3.0 mg mL^{-1} and the mixtures were sonicated for 3 h. To prepare MoS_2–graphene composites, 4 parts MoS_2 dispersion was mixed with 1 part graphene dispersion and then the mixtures were sonicated for further 2 h. The resulting dispersions were centrifuged at 10,000 rpm for 1 h and the precipitates were collected, re-dispersed in methanol, filtrated, washed copiously with methanol, and dried at 100 °C for 12 h. The obtained products were denoted as exfoliated MoS_2, MoS_2/GnP and MoS_2/CCG corresponding to the samples without graphene, with GnP or CCG, respectively.

2.4. Characterization

The morphology of MoS_2–graphene composites was characterized by scanning electron microscopy (SEM, JEOL JSM-6500 FE). XRD patterns were analyzed on a Rigaku D/MAZX 2500V/PC high power diffractometer using Cu Kα radiation (k = 1.5418 Å). The textural properties were measured by means of N_2 sorption analysis on a Micromeritics ASAP 2010 apparatus (USA).

2.5. Electrochemical measurements

The electrochemical characterization for lithium storage capabilities was performed through coin half-cells (CR2016-type) with the working electrode containing exfoliated MoS_2, MoS_2/GnP, MoS_2/CCG, and a lithium metal counter electrode. The electrolyte was 1 M $LiPF_6$ (Panaxetec Co., Korea) dissolved in ethylene carbonate:dimethyl carbonate:ethyl methyl carbonate (1:1:1 by volume). The working electrodes were prepared by a slurry coating procedure. The slurry consisted of 80 wt% active material, 5 wt% vapor grown carbon fiber as conducting material and 15 wt% polyvinylidene fluoride as binder (Solef 50130, Solvey Co.). The slurry was spread on copper foil, which acted as a current collector. The coated electrodes were dried at 110 °C for 12 h under vacuum and were then pressed.

The fabricated coin half-cells were aged for 24 h to provide uniform electrolyte permeation into active material and were then galvanostatically discharged to 5 mV and charged to 3.0 V at a constant current of 100 mA g^{-1} for 50 cycles (WBCS3000, WonAtech, Korea). Cyclic voltammetry (CV, Biologis, VSP) tests were conducted from 0 V to 3.0 V at a scan rate of 0.5 mV s^{-1}. In addition, electrochemical impedance spectroscopy (EIS) tests were performed in a frequency range of 100 kHz to 0.01 Hz at a scan rate of 0.5 mV s^{-1}.

3. Results and discussion

3.1. Morphology and structure of exfoliated MoS_2 and MoS_2–graphene composites

Two kinds of graphenes were chosen to prepare MoS_2–graphene composites including commercial graphene nanoplatelet (GnP) and chemically converted graphene (CCG). GnP is mechanically exfoliated graphene which has very low oxygen content, less than 1.0 wt % [26]. With the average thickness around 6 μm, GnP is easier to exfoliate to single and few-layered flakes than graphite. In contrast, CCG was prepared by hydrazine reduction of graphene oxide at low temperature, which still possessed many oxygen functional groups, leading to high dispersibility in polar organic solvent such as NMP [25].

The morphologies of commercial MoS_2, exfoliated MoS_2 and MoS_2–graphene composites characterized by SEM are shown in Fig. 1 and Fig. S1 (see Supplementary data). Fig. 1a clearly shows that the commercial MoS_2 flakes have a layered structure with the lateral size from few to tens of μm and a thickness from hundreds of nm to μm. After liquid-phase exfoliation by sonication for 6 h, the MoS_2 flakes are much thinner and smaller in lateral size. Most MoS_2 flakes are smaller than 2 μm and the thicknesses are around tens of nm (Fig. 1b). The exfoliated MoS_2 flakes are much thicker than single or few-layered flakes, implying the restacking of single and few-layered flakes during the centrifugation, filtration and drying processes. Although the restack occurred, the size and thickness of exfoliated MoS_2 flakes were much smaller than those of pristine MoS_2. The morphology of MoS_2/GnP showed that both of MoS_2 and GnP flakes were very thin and it was hard to distinguish MoS_2 flakes from GnP flakes due to their similar structure (Fig. 1c). However, the SEM EDS mapping in Fig. 1e reveals that the 4 elements (including Mo, S, C and O) were homogeneously distributed, indicating that MoS_2 and GnP flakes were homogeneously mixed. For MoS_2/CCG (Fig. 1d), since CCG can be easily exfoliated to a single layer in polar solvent [24], the large, thin, crumpled and wrinkled sheets originated from the CCG sheets, while the small, thin and flat flakes are from MoS_2 flakes. SEM EDS mapping shows the homogenous distribution of both MoS_2 flakes and CCG sheets. In both

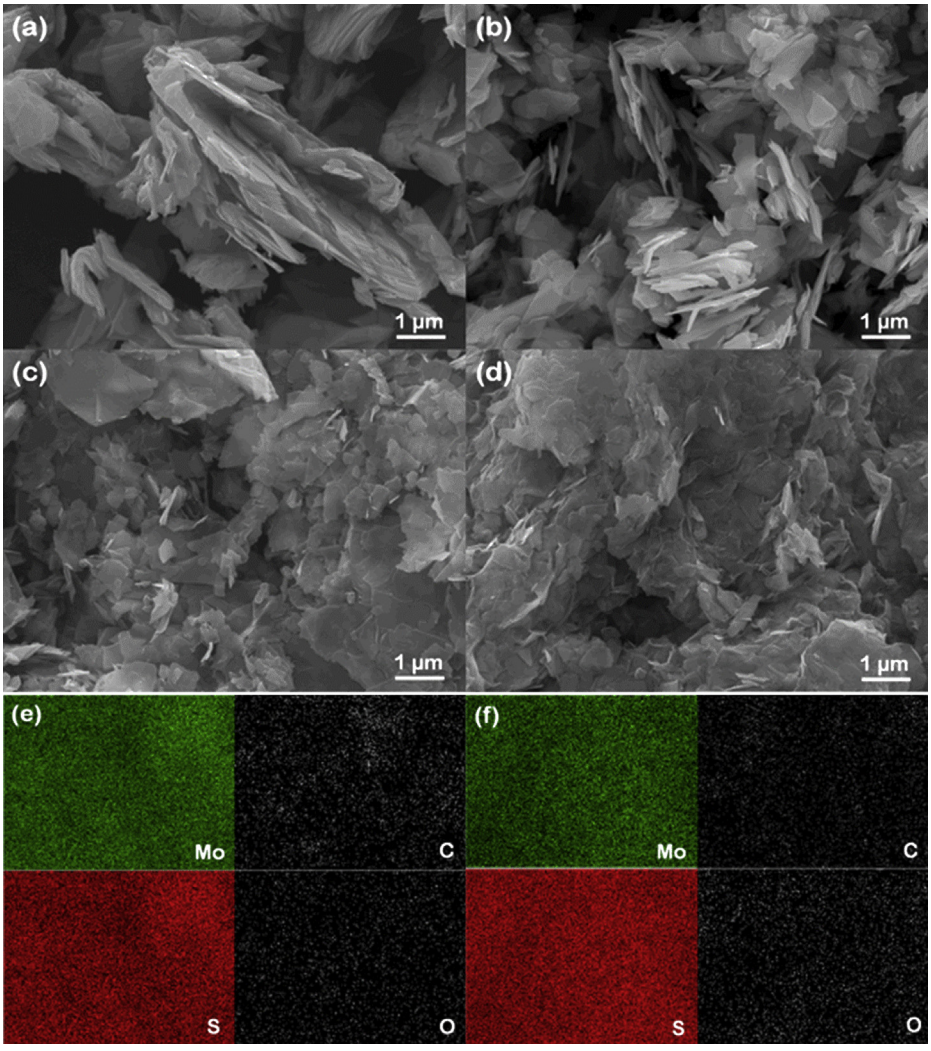

Fig. 1. SEM images of (a) pristine MoS_2, (b) exfoliated MoS_2, (c) MoS_2/GnP and (d) MoS_2/CCG; (e) and (f) SEM EDS mapping of (c) and (d), respectively.

MoS_2–graphene composites, thick MoS_2 flakes were not observed, indicating that the presence of graphene sheets effectively prevent the restack of MoS_2 flake during processing.

The exfoliation of MoS_2 and graphene was further characterized by XRD (Fig. 2). XRD patterns of commercial MoS_2 showed a series of strong and sharp peaks assigned to the {002}, {004}, {100}, {103} and {006} reflections of hexagonal MoS_2, which are in accordance with those established by JCPDS card number 37-1492, indicating that commercial MoS_2 is highly crystalline. After exfoliation, the primary {002} diffraction peak at 14.46 °C, corresponding to a *d*-spacing of 0.62 nm, sharply decreased, indicating that the thickness of MoS_2 flakes greatly decreased. Co-exfoliation of MoS_2 and graphene resulted in a further decrease in the intensity of the {002} diffraction peak, implying that the presence of graphene sheets effectively prevent restacking of MoS_2 flakes, which is consistent with the SEM observations. The XRD patterns of MoS_2/GnP and MoS_2/CCG show that the intensity of the {002} diffraction peak in MoS_2/CCG is significantly lower than that of MoS_2/GnP, indicating that CCG has a higher efficiency in preventing restacking of MoS_2. Moreover, the XRD pattern of MoS_2/GnP exhibited a small peak at 26.5 °C, corresponding to a *d*-spacing of 0.34 nm, which can be attributed to the {002} diffraction peak of graphite [27]; this demonstrates that GnP was not fully exfoliated to a single layer. The efficient prevention of MoS_2 restacking in combination of CCG can be explained by the complete exfoliation of CCG in NMP [24] and the good interaction between CCG sheets and MoS_2 flakes. With an oxygen content of 13.7 wt% [25], CCG possesses many oxygen functional groups which may have a high chemical affinity with the polar surface of MoS_2 flakes [28], leading to interfere with restacking of MoS_2 flakes. Raman spectra in Fig. S3 show that the characteristic peaks of MoS_2 significantly red-shifted in presence of graphene, especially for CCG, which is an indication of the strong interaction between CCG and MoS_2 flakes.

Nitrogen adsorption–desorption isotherms are further used to investigate the effects of the exfoliation of MoS_2 on the pore structure and specific surface area of MoS_2 and MoS_2–graphene composites (Fig. 3a). The commercial MoS_2 and exfoliated MoS_2 exhibit reversible type II isotherms, which indicate non-porous material. In contrast, MoS_2/GnP and MoS_2/CCG exhibit a typical IV isotherm with the typical H2 hysteresis loop, which is an indication of a typical mesoporous material. The BET specific surface area (SSA) in Table 1 shows that after exfoliation, SSA of exfoliated MoS_2 is nearly 3 times increased in comparison to that of pristine MoS_2 and about 2 times higher than that of MoS_2 restacked from aqueous suspension of exfoliated MoS_2 [8]. The SSA of MoS_2/GnP and MoS_2/CCG is about 2 times higher than that of exfoliated MoS_2, which can be explained by a combination of high graphene surface area (the theoretical SSA of graphene is 2630 $m^2\ g^{-1}$) and better exfoliation of MoS_2. Moreover, the pore volume of MoS_2/GnP and MoS_2/CCG greatly increased compared to that of exfoliated MoS_2. Fig. 3b shows the pore size distribution of MoS_2 and MoS_2–graphene composites. MoS_2/CCG has a broad pore size distribution, from 3 nm up to nearly 40 nm, which is created from the crumple and wrinkles in CCG sheets. The large pore volume and pore size are desirable for electrode materials because they create a pathway for electrolyte ions to access active material and tolerate the volume expansion of active material during the lithiation/delithiation process.

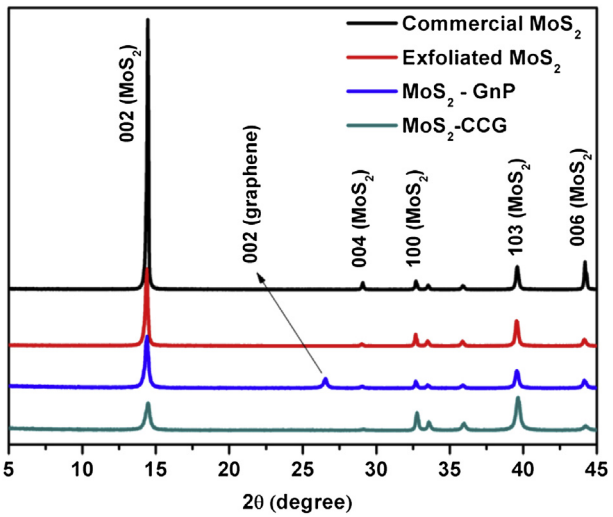

Fig. 2. XRD patterns of MoS_2 and MoS_2–graphene composites.

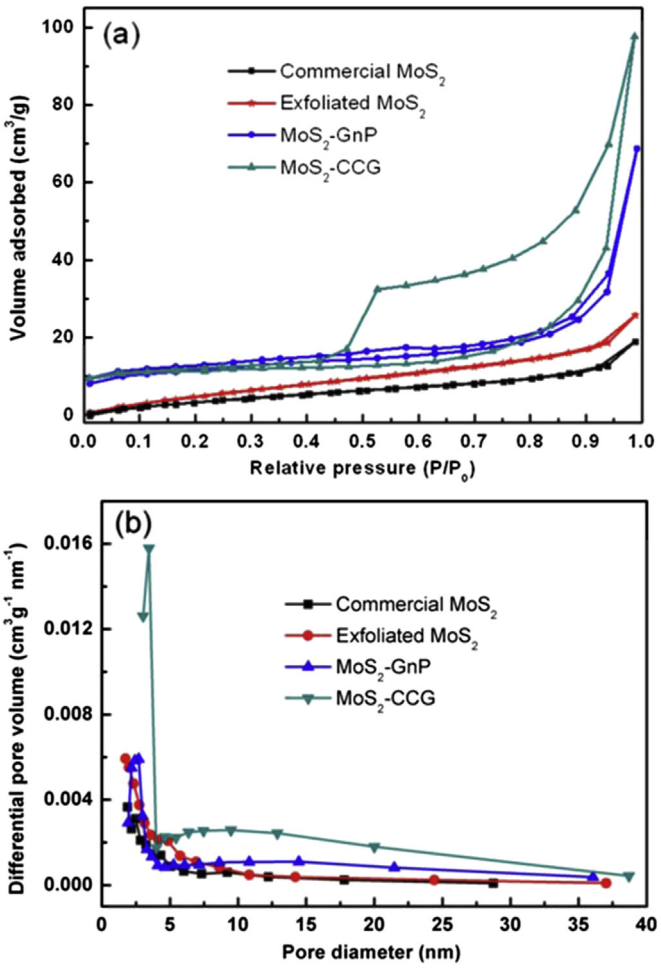

Fig. 3. (a) Nitrogen adsorption isotherm and (b) pore size distribution of the MoS_2 and MoS_2–graphene composites.

Table 1
Specific surface area and pore volume of MoS_2 and MoS_2–graphene composites.

	BET specific surface area ($m^2\ g^{-1}$)	Pore volume ($cm^3\ g^{-1}$)
Commercial MoS_2	7.1	0.026
Exfoliated MoS_2	20.5	0.036
MoS_2–GnP	39.1	0.102
MoS_2–CCG	37.8	0.193

3.2. Electrochemical performance

Fig. 4 shows the first three charge and discharge curves and cyclic voltammetry of exfoliated MoS_2, MoS_2/GnP and MoS_2/CCC. The first discharge and charge capacities of exfoliated MoS_2 are 706 and 455 mA h g^{-1}, respectively, corresponding to 64.4% coulombic efficiency (Fig. 4a). The discharge capacity of exfoliated MoS_2 is significantly higher than that of bulk MoS_2 in previous reports (525–600 mA h g^{-1}) [9,14], indicating that the exfoliation of bulk MoS_2 into small and thin MoS_2 flakes leads to an improvement in specific capacity. The high surface area of exfoliated MoS_2 facilitates the access of Li^+ ions during the lithiation process. However, the discharge capacity of exfoliated MoS_2 decreased sharply to 475 mA h g^{-1} in the second cycle, suggesting poor reversibility of Li^+ ions in the exfoliated MoS_2, which is similar to the phenomenon observed in bulk MoS_2 [9]. Thereby, most of Li^+ ions are trapped in the unexfoliated structure after the first discharge.

The first discharge capacities of MoS_2/GnP and MoS_2/CCG are 780 and 957 mA h g^{-1}, respectively, which are much higher than that of exfoliated MoS_2. The higher first discharge capacity of MoS_2–graphene composites can be explained by better exfoliation of MoS_2 flakes as discussed above. More importantly, the capacity of MoS_2–graphene composites did not rapidly degrade like exfoliated MoS_2. The charge capacities of both MoS_2/GnP and MoS_2/CCG increased about 5% in second and third cycles (Fig. 4c and e).

The first discharges of all samples exhibit two potential plateaus at about 1.0 and 0.6 V. The first plateau at 1.0 V is indicative of the formation of Li_xMoS_2, and the plateau variation in the lithium intercalation is attributed to different defect sites of MoS_2 [9,10,16–18]. The long plateau at 0.6 V can be attributed to the conversion reaction process related to the reduction of MoS_2 to Mo metal accompanied by the formation of Li_2S [9,16]. In the second and third cycles, the plateaus at 1.0 and 0.6 V in the first discharge are absent, whereas another, new plateau at 1.7 V for exfoliated MoS_2 and 2.1 V for MoS_2–graphene composites appeared. In the first charge shown in Fig. 4a, c and e, a potential plateau at 2.2 V was observed, which is related to the oxidation of Li_2S into sulfur [16]. However, in the subsequent cycles of exfoliated MoS_2, this plateau disappeared due to the fading of the electrode.

The electrochemical properties of exfoliated MoS_2 and MoS_2–graphene composites were further investigated by cyclic voltammetry. As shown in Fig. 4b, d and f, the first cycles of all samples exhibit two broad peaks centered at 0.65 and 0.25 V in the cathodic sweep. The first peak at 0.65 V can be attributed to the coordination of Mo by six S atoms (i.e., MoS_6), which changes from a trigonal prismatic to an octahedral structure while Li^+ ions intercalate into MoS_2

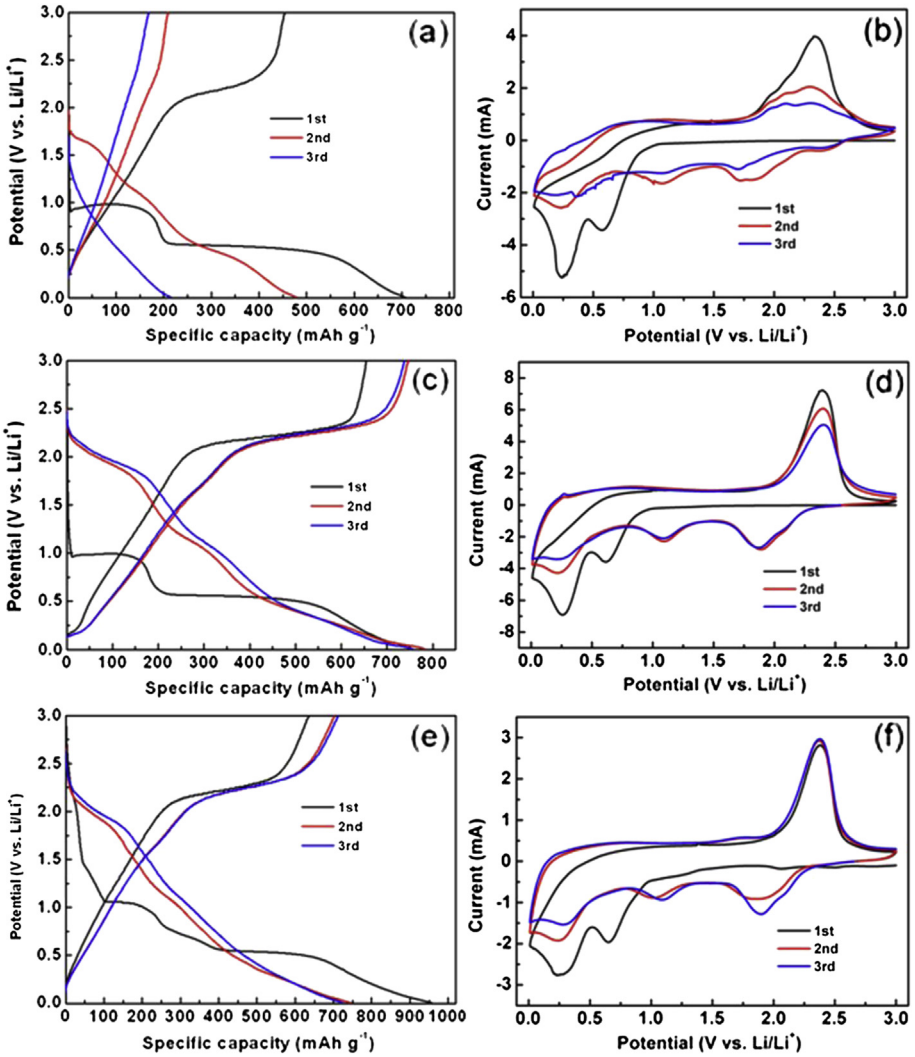

Fig. 4. (a), (c) and (e) First three charge–discharge curves and (b), (d) and (f) cyclic voltammetry of exfoliated MoS_2, MoS_2/GnP and MoS_2/CCG, respectively.

layers, thus forming Li_xMoS_2 ($x = 3–4$) [6,11,16]. The second peak at 0.25 V is indicative of the reduction of Mo^{4+} to Mo metal, accompanied by the formation of Li_2S according to $Li_xMoS_2 \rightarrow Mo + Li_2S$ [6,11,16]. In the first anodic sweep, only one peak centered at 2.4 V was observed for all samples, corresponding to the oxidation of Li_2S into sulfur [16]. Xiao et al. [16] used XRD in combination with HR-TEM associated with selected-area electron diffraction (SAED) to study electrode structure after the first cycle and found that the electrode is a mixture of S and Mo instead of the original MoS_2. This explained why the peak centered at 0.65 V in the first cathodic sweep disappears and two new peaks at 1.9 and 1.1 V are observed in the following sweeps. The peak at 1.9 V can be attributed to the conversion of element S_8 to polysulfides and then to Li_2S [16]. In the following anodic sweeps, the intensity of a peak at 2.4 V for exfoliated MoS_2 and MoS_2/GnP gradually decreases, indicating the fading of the electrode. In contrast, the intensity of this peak of MoS_2/CCG even though increasing slightly, demonstrates excellent reversibility and cyclability.

Fig. 5 shows the cyclic behavior of the exfoliated MoS_2 and MoS_2–graphene composites at density of 100 mA g^{-1}. It can be seen that a capacity of 706 mA h g^{-1} is delivered during the first discharge process, but the capacity sharply drops to only 215 mA h g^{-1} after three cycles and then to 55 mA h g^{-1} after 50 cycles. MoS_2/GnP shows better cyclic performance with the first discharge capacity up to 780 mA h g^{-1}, then the capacity gradually decreases to 225 mA h g^{-1} after 50 cycles. In contrast, MoS_2/CCG exhibits excellent cyclic stability. MoS_2/CCG exhibits a discharge capacity of 957 mA h g^{-1} in the first cycle, which drops to 744 and 710 mA h g^{-1} for the second and tenth cycles, respectively, but then slightly increases to 750 mA h g^{-1} after 50 cycles, which is comparable to MoS_2/PEO/graphene composites in previous reports [16]. The fast decrease in capacity of exfoliated MoS_2 and MoS_2/GnP can be explained by the trapping of Li^+ ions in the thick and unexfoliated MoS_2 flakes, resulting in poor reversibility. Moreover, it is well known that the volume change of active materials during lithiation/delithiation may be another factor affecting the cycle stability of the electrodes [6]. As discussed above, the exfoliated MoS_2 is a non-porous material while MoS_2/GnP is a mesoporous material, but pore volume and pore size are very small, which may not be enough to tolerate the volume change during the lithiation/delithiation process. In contrast, MoS_2/CCG is a highly mesoporous material consisting of thin MoS_2 flakes and crumpled and wrinkled CCG which created large pore volumes and pore sizes. The capacities and cyclic stability of exfoliated MoS_2, MoS_2/GnP and MoS_2/CCG are highly consistent with their morphology and structure.

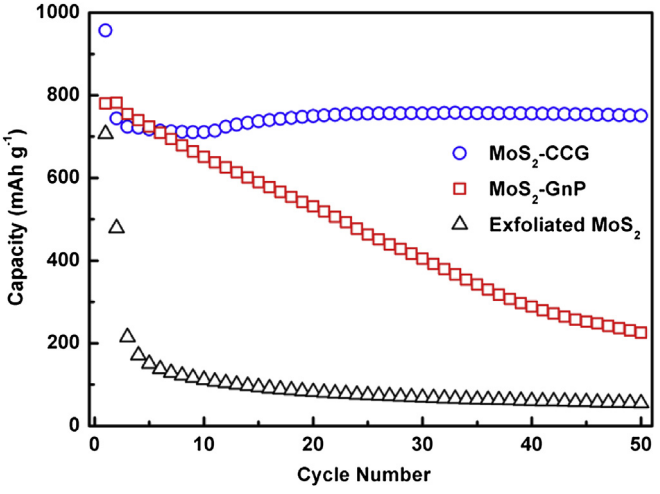

Fig. 5. Cyclic behavior of exfoliated MoS_2, MoS_2/GnP and MoS_2/CCG.

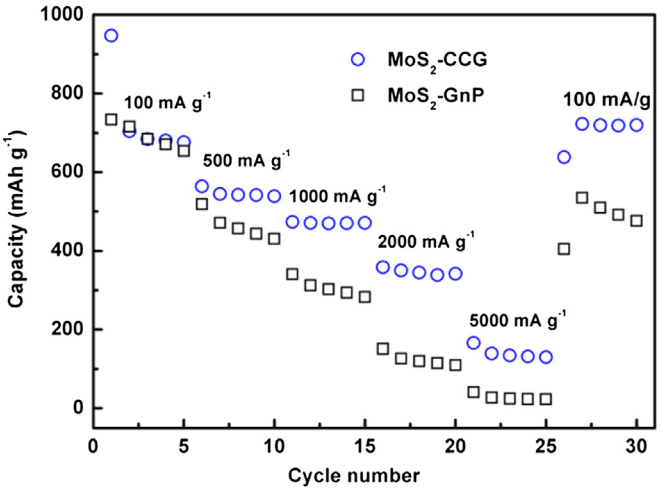

Fig. 6. Rate capacity of MoS_2–graphene composites at different current densities.

Fig. 6 shows the rate capacity of MoS_2–graphene composites. It can be seen that MoS_2/CCG exhibits excellent rate capacity with a reversible capacity as high as 700 mA h g^{-1} after the 5th cycle at a current density of 100 mA g^{-1}, then 470 mA h g^{-1} after the 15th cycle at 1000 mA g^{-1} and 342 mA h g^{-1} at the 20th cycle at 2000 mA g^{-1}. The good retentions of 67 and 49% are obtained when the current density increases 10 and 20 times, respectively. More importantly, when the rate returns from 5000 mA g^{-1} to the initial 100 mA g^{-1}, the capacity can be restored to 720 mA h g^{-1}, which is even a little higher than that at the 5th cycle, indicating the excellent rate performance.

4. Conclusions

We report a facile method to prepare a MoS_2–graphene composite by liquid phase co-exfoliation of highly crystalline MoS_2 with two kinds of graphene, GnP and CCG. Although restacking occurred during processing, the size and thickness of exfoliated MoS_2 flakes are much smaller than that of bulk MoS_2. The combination of SEM, XRD and BET results reveal that the MoS_2–graphene composites are mesoporous materials consisting of very thin MoS_2 flakes and graphene sheets. MoS_2 in the composite with CCG has better exfoliation degree due to its good interaction with highly dispersed, oxygenated CCG sheets. The prepared MoS_2–graphene composites display good performance as anode materials for lithium ion batteries. Exfoliation of the MoS_2 is the key factor for high electrochemical lithiation/delithiation performance. The MoS_2/CCG composite exhibited best performance with a first discharge capacity more than 950 mA h g^{-1} and 750 mA h g^{-1} after the 50th cycle. Moreover, MoS_2/CCG also exhibits a high rate capacity with a reversible capacity more than 350 mA h g^{-1} at a rate as high as 2000 mA g^{-1}, recovering to more than 720 mA h g^{-1} at a rate of 100 mA g^{-1}. The present results suggest that liquid phase co-exfoliation of commercial MoS_2 and CCG is a promising approach to prepare MoS_2–graphene composites for LIB applications. We believe that there is still more room for improving the performance of MoS_2/CCG by optimizing the exfoliation time and the ratio of MoS_2 and CCG.

Acknowledgment

This research was financially supported by the Ministry of Knowledge Economy (MKE), Korea Institute for Advancement of Technology (KIAT) through the Inter-ER Cooperation Projects.

Appendix A. Supplementary data

Supplementary data associated with this article can be found in the online version, at http://dx.doi.org/10.1016/j.jpowsour.2013.01.053.

References

[1] M.S. Whittingham, Chem. Rev. 104 (2004) 4271–4301.
[2] J.B. Goodenough, Yongsik Kim, Chem. Mater. 22 (2010) 587–603.
[3] R. Marom, S.F. Amalraj, N. Leifer, D. Jacob, D. Aurbach, J. Chem. Mater. 21 (2011) 9938–9954.
[4] A. Manthiram, J. Phys. Chem. Lett. 2 (2011) 176–184.
[5] Y. Miki, D. Nakazato, H. Ikuta, T. Uchida, M. Wakihara, J. Power Sources 54 (1995) 508–510.
[6] H. Li, W. Li, L. Ma, W. Chen, J. Wang, J. Alloys Compd. 471 (2009) 442–447.
[7] C. Feng, J. Ma, H. Li, R. Zeng, Z. Guo, H. Liu, Mater. Res. Bull. 44 (2009) 1811–1815.
[8] G. Du, Z. Guo, S. Wang, R. Zeng, Z. Chen, H. Liu, Chem. Commun. 46 (2010) 1106–1108.
[9] J. Xiao, D. Choi, L. Cosimbescu, P. Koech, J. Liu, J.P. Lemmon, Chem. Mater. 22 (2010) 4522–4524.
[10] K. Chang, W. Chen, L. Ma, H. Li, H. Li, F. Huang, Z. Xu, Q. Zhang, J.-Y. Lee, J. Mater. Chem. 21 (2011) 6251–6257.
[11] H. Hwang, H. Kim, J. Cho, Nano Lett. 11 (2011) 4826–4830.
[12] M. Liang, L. Zhi, J. Mater. Chem. 19 (2009) 5871–5878.
[13] J. Hou, Y. Shao, M.W. Ellis, R.B. Moore, B. Yi, Phys. Chem. Chem. Phys. 13 (2011) 15384–15402.
[14] E.J. Yoo, J. Kim, E. Hosono, H. Zhou, T. Kudo, I. Honma, Nano Lett. 8 (2008) 2277–2282.
[15] G. Wang, X. Shen, J. Yao, J. Park, Carbon 47 (2009) 2049–2053.
[16] J. Xiao, X. Wang, X.Q. Yang, S. Xun, G. Liu, P.K. Koech, L. Liu, J.P. Lemmon, Adv. Funct. Mater. 21 (2011) 2840–2846.
[17] K. Chang, W. Chen, Chem. Commun. 47 (2011) 4252–4254.
[18] K. Chang, W. Chen, ACS Nano 5 (2011) 4720–4728.
[19] Y. Hernandez, V. Nicolosi, M. Lotya, F.M. Blighe, Z. Sun, S. De, I.T. McGovern, B. Holland, M. Byne, Y.K. Gun'ko, J. Boland, P. Niraj, G. Duesberg, S. Krishnamuthy, R. Goodhue, J. Hutchinson, V. Scardaci, A.C. Ferrari, J.N. Coleman, Nat. Nanotechnol. 3 (2008) 563–568.
[20] U. Khan, A. O'Neill, M. Lotya, S. De, J.N. Coleman, Small 6 (2010) 864–871.
[21] U. Khan, H. Porwal, A. O'Neill, K. Nawaz, P. May, J.N. Coleman, Langmuir 27 (2011) 9077–9082.
[22] J.N. Coleman, M. Lotya, A. O'Neil, S.D. Bergin, P.J. King, U. Khan, K. Young, A. Gaucher, S. De, R.J. Smith, I.V. Shvets, S.K. Arora, G. Stanton, H.-Y. Kim, K. Lee, G.T. Kim, G.S. Duesberg, T. Hallam, J.J. Boland, J.J. Wang, J.F. Donegan, J.C. Grunlan, G. Moriarty, A. Shmeliov, R.J. Nicholls, J.M. Perkins, E.M. Grieveson, K. Theuwissen, D.W. McComb, P.D. Nellist, V. Nicolosi, Science 331 (2011) 568–571.
[23] A. O'Neill, U. Khan, J.N. Coleman, Chem. Mater. 24 (2012) 2414–2421.
[24] V.H. Pham, T.T. Dang, T.V. Cuong, S.H. Hur, B.-S. Kong, E.J. Kim, J.S. Chung, Korean J. Chem. Eng. 29 (2012) 680–685.
[25] T.T. Dang, V.H. Pham, S.H. Hur, E.J. Kim, B.-S. Kong, J.S. Chung, J. Colloid Interface Sci. 376 (2012) 91–96.
[26] http://www.xgsciences.com/products.html (website was last accessed on July 11, 2012).
[27] M.J. McAllister, J.-L. Li, D.H. Adamson, H.C. Schniepp, A.A. Abdala, J. Liu, M. Herrera-Alonso, D.L. Milius, R. Car, R.K. Prud'homme, I.A. Aksay, Chem. Mater. 19 (2007) 4396–4404.
[28] J. Heising, F. Bonhomme, M.G. Kanatzidis, J. Solid State Chem. 139 (1998) 22–26.